Journal of Alloys and Compounds 513 (2012) 487–494

Contents lists available at SciVerse ScienceDirect

Journal of Alloys and Compounds

journal homepage: www.elsevier.com/locate/jallcom

Thermodynamic quantities and oxygen nonstoichiometry of undoped $BaTiO_{3-\delta}$ by thermogravimetric analysis

M.-B. Choi, S.-Y. Jeon, H.-N. Im, S.-J. Song*

Department of Materials Science and Engineering, Chonnam National University, 300 Yongbong-dong, Buk-gu, Gwangju 500-757, South Korea

ARTICLE INFO

Article history:
Received 26 August 2011
Received in revised form 27 October 2011
Accepted 28 October 2011
Available online 7 November 2011

Keywords:
Thermogravimetry
Nonstoichiometry
Thermodynamic quantities

ABSTRACT

Thermogravimetry analysis was performed to determine the oxygen nonstoichiometry of oxides by using a home-made experimental set-up with Cahn D200 microbalance for an undoped $BaTiO_{3-\delta}$ specimen. The relative partial molar enthalpy and entropy of oxygen for undoped $BaTiO_{3-\delta}$ were also calculated from the slope and intercept of the $\delta - P_{O_2} - T$ relation, respectively. The negative signs of partial molar enthalpy and entropy in the oxygen deficient regime indicated that the incorporation of oxygen is an exothermic process. The values for K_i and K_{Re} of the undoped $BaTiO_{3-\delta}$ are best described by the following equations:

$$K_i/\mathrm{cm}^{-6} = (1.69 \pm 1.51) \times 10^{46} \exp\left(-\frac{2.93 \pm 0.23\,\mathrm{eV}}{kT}\right)$$

$$K_{Re}/\mathrm{cm}^{-9} = (7.15 \pm 5.55) \times 10^{73} \exp\left(-\frac{5.80 \pm 0.15\,\mathrm{eV}}{kT}\right)$$

The difference in n–p transition P_{O_2} compared with reference should be further understood by identifying the cation nonstoichiometry and the value of impurity defects for the clarification of defect structure.

1. Introduction

It has long been the basic rule of solid state ionics that both the transport and thermodynamic properties of the oxide utilized in electrochemical applications are strongly influenced by the nature of the defect system of oxides that should be subjected to the external thermodynamic conditions [1,2]. Chemical potentials may be assigned to all elements in redox reactions involving the structure elements of oxide and equilibrium conditions are formulated when the free energy change of the reaction equals the difference of the sums of chemical potentials of elements at the product and reactant sides of the reaction [3]. Because mass action law defines the relationship between oxygen partial pressure (P_{O_2}) and the defect concentration in crystal oxides during redox reactions, much interest has been focused on precisely how to extract the internal/external reaction constants from various experimental measurements. Several defect-related transport properties, including optical, electrical, and electrochemical measurements, have been applied to obtain the thermodynamic quantities of oxides [4–7].

Among these techniques, thermogravimetric analysis (TGA) has been recognized as one of the most valuable tools for directly clarifying the defect concentrations of oxides as a function of the thermodynamic control parameters by measuring the weight change of oxide caused by the redox reactions until it reaches a new equilibrium state determined by the change of thermodynamic conditions such as temperature and P_{O_2} [8–10]. The weight change can then be directly converted into the corresponding variation of oxygen nonstoichiometry, δ, of the oxide specimen. However, despite the clarity in TGA's working principles, its application to determine the oxygen nonstoichiometry has not been considered a trivial matter. Moreover, because the weight change undergoing redox reactions may be interfered with by multiple spurious weight changes caused by environmental and structural factors, the exact measurement of the pure weight change by redox reactions from oxides has been recognized as a critical hurdle that must be overcome, especially in the case of very narrow oxygen stoichiometric oxides. Especially, for the perovskite oxides showing n- to p-type transition in an extended range of P_{O_2} at elevated temperature, the nonstoichiometric variation with P_{O_2} is expected to be so negligible

* Corresponding author at: School of Materials Science and Engineering, Chonnam National University, 300 Yongbong-dong, Buk-Gu, Gwangju, 500-757, South Korea. Tel.: +82 62 530 1706; fax: +82 62 530 1699.
E-mail address: song@chonnam.ac.kr (S.-J. Song).

0925-8388/$ – see front matter © 2011 Elsevier B.V. All rights reserved.
doi:10.1016/j.jallcom.2011.10.096

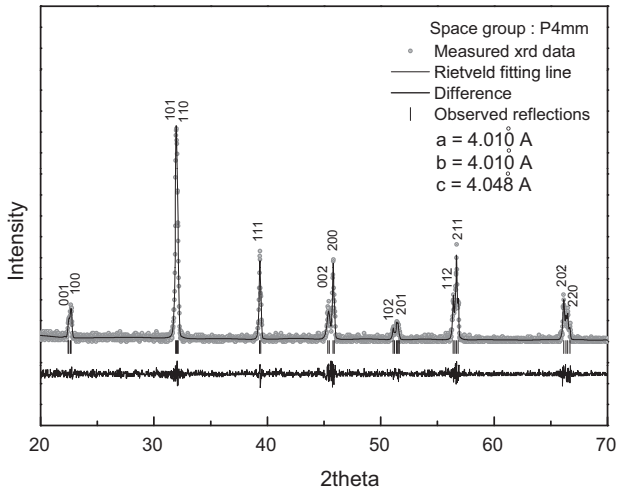

Fig. 1. Room temperature X-ray diffraction (XRD) patterns of $BaTiO_{3-\delta}$.

(corresponding to around several micrograms difference in weight) in the electron/hole mixed conduction regions that only a few TGA has been successful due to the difficulty in experimental resolution [11].

In this work, we report a newly built, home-made experimental set-up consisting of an asymmetric TGA system with Cahn D200 microbalance and is then applied to evaluate the thermodynamic quantities and oxygen nonstoichiometry of $BaTiO_{3-\delta}$ as a function of temperature ($1073 \leq \mathrm{Temp/K} \leq 1273$) and P_{O_2} ($-18 \leq \log P_{O_2}/\mathrm{atm} \leq 0$) corresponding to the very narrow oxygen nonstoichiometric change ($\approx 10^{-4}$ mol). On the basis of the defect chemistry widely discussed in the literature, the nonstoichiometry, δ, was successfully determined with non-linear functional fitting. Furthermore, the relative partial molar enthalpy and entropy of oxygen for undoped $BaTiO_{3-\delta}$ were also calculated from the slope and intercept of the $\delta - P_{O_2} - \mathrm{T}$ relation,

2. Experimental

2.1. Sample preparation

"Undoped" polycrystalline $BaTiO_{3-\delta}$ specimens were prepared by conventional solid state reaction method. The starting materials of $BaTiO_{3-\delta}$ (Alfar Aesar, 99.99%) in powder form were pressed into pellets, cold-isostatic-pressed, and sintered at 1623 K for 5 h in air. It should be mentioned that 5 ppm of Fe and Al by weight were identified as impurities based on the certificate of analysis given by company. During the sintering, these $BaTiO_{3-\delta}$ specimens on a first-layer $BaTiO_{3-\delta}$ substrate were fully covered by $BaTiO_{3-\delta}$ starting powders to prevent any possible reaction. The densities of the resultant disks were 90% of the theoretical values. X-ray diffraction (XRD) spectra confirmed the single phase tetragonal $BaTiO_{3-\delta}$ (space group, *P4mm*) as shown in Fig. 1, in agreement with the literature [12,13]. The specimens for TG measurements were cut out of the sintered disk into around 781 mg cylinder. Because the oxygen nonstoichiometry of yttria-stabilized zirconia (YSZ) does not need to be considered like the coulometric titration measurements, relatively light, 781 mg specimens were prepared.

2.2. Experimental set-up

TGA determines the weight change of a specimen in relation to the change in P_{O_2} and temperature. Therefore, such analysis relies on a high degree of precision in three measurements: weight, P_{O_2}, and temperature change. The experimental apparatus of asymmetric TGA with Cahn D200 microbalance that was used to make these three precise measurements is shown in Fig. 2. Spurious weight changes caused by the thermal convection flow within the reactor are mainly ascribed to the temperature difference along the hang-down wire [14]. To minimize the thermal convection flow reaching the specimen and causing some disturbance to the specimen, a home-made reflector was designed. The plausible electrostatic effect of the microbalance due to the application of friction to the gas flow was minimized by using the metal end-cap connected to a ground connection [15]. To minimize the thermal diffusion due to the difference in the thermal diffusivity of the component gases, 90% ultra-high purity (UHP) N_2 carrier gas was used and the mixture gas was produced by flowing through a mixing bath zone [16,17]. The radiation effect due to the asymmetric design of TGA was minimized by placing an oval mirror inside the tube connected to the microbalance [11]. The input power stability was assured by using a constant voltage, constant current, uninterruptible power supplier. The inherent effects due to the asymmetric design of TGA, including upthrust buoyancy [17,18], thermomolecular force [17], and high-temperature aerodynamic effects [15,19], were corrected by subtracting the spurious weight change of a dummy test with alumina from the real measurements. The flow of the N_2 protective gas through a counter weight reactor prevents any corrosive gas flow into the microbalance. The effects from the reactor tube size and hang-down wire diameter were also considered in our experimental design. To minimize the temperature variation near the microbalance and balance controller, a temperature-programmed heater and air conditioner were used. Finally, the vibration effect, one of the most important and serious obstacles to high resolution, was relieved by using a two-step, anti-vibration pad on a 200 kg metal ground pad.

The P_{O_2} was controlled by a N_2/O_2 gas mixture at higher P_{O_2} and a CO/CO_2 gas mixture at lower P_{O_2}, with UHP N_2 carrier gas at a constant flow rate of 180 sccm, while the total flow rate of the gas mixture to the reactor was maintained at 200 sccm for all measurements. Each gas flow during the TG measurements was controlled with a mass flow controller (MKS) and the rate was measured with a flow calibrator (Digital flowmeter, Optiflow 570). The equilibrium P_{O_2} was determined from the open circuit potential of a YSZ-based oxygen sensor after the reactor and near the specimen within the reactor. The temperature of oxygen sensor located in outside of reactor was maintained as same as the reactor temperature, maintained within 1 K of the target temperature. The both YSZ oxygen sensors calibrated in terms of standard gas and temperature.

The relationship between the oxygen nonstoichiometric variation and the measured weight change can be described as

$$\Delta\delta = \frac{\Delta w}{M_O}\frac{M_S}{w_S} \tag{1}$$

by assuming that only oxygen exchange from the specimen occurs and changes the specimen weight, where $\Delta\delta$ is the oxygen nonstoichiometric variation, Δw the weight change of the specimen, w_S the initial specimen weight, M_O the oxygen atomic weight, and M_S denotes the molecular formula weight of the specimen.

3. Results and discussion

After subtracting the spurious weight change due to the many factors described in experimental section, Fig. 3 shows a typical weight change profile upon oxidation and reduction as a function of time for the $BaTiO_{3-\delta}$ specimen with ± 0.5 μg resolution, in which the measured relative weight change of around 3 μg corresponds to an oxygen nonstoichiometric change of less than around 10^{-4} mol. Our TGA system was able to clearly distinguish the oxygen nonstoichiometric change of less than 10^{-4} mol for the $BaTiO_{3-\delta}$ specimen at 1273 K with 200 sccm total gas flow dynamic condition with ± 1.5 μg resolution in the worst case over all the measurement ranges. By cyclic operation of oxidation and reduction at a given temperature, we confirmed the reproducibility of the measurement by demonstrating its return to the starting values.

Despite the debate regarding the electrically compensating defect species for oxygen vacancies, especially about cation defects, the absolute nonstoichiometry of undoped $BaTiO_{3-\delta}$ was successfully extracted from the coulometric titration measurements based on defect chemical rationale by considering acceptor-type impurities, where n- to p-type transition occurs [20,21]. One should note that the analysis of absolute nonstoichiometry of undoped $BaTiO_{3-\delta}$ was also successful based on Schottky-Wager disorder [22]. With only P_{O_2} dependence of the mass changes from TGA, the majority defects species may not be clarified especially within *n–p* transition regime due to the same oxygen partial pressure dependence of oxygen vacancy concentration, regardless of cation defect or acceptor impurity. Therefore, the oxygen nonsotichiometry caused from the variation of cation ratio, Ba/Ti, was not considered in this work to make the analysis simple as possible, and one may define the external and internal equilibria as

$$O_O^x = V_O^{\bullet\bullet} + 2e^{/} + \frac{1}{2}O_2(g); \quad K_{Re} = [V_O^{\bullet\bullet}]n^2 P_{O_2}^{1/2} \tag{2}$$

$$0 = e^{/} + h^{\bullet}; \quad K_i = n \cdot p \tag{3}$$

Fig. 2. Experimental set-up of thermogravimetric analysis (TGA) with Cahn microbalance D-200.

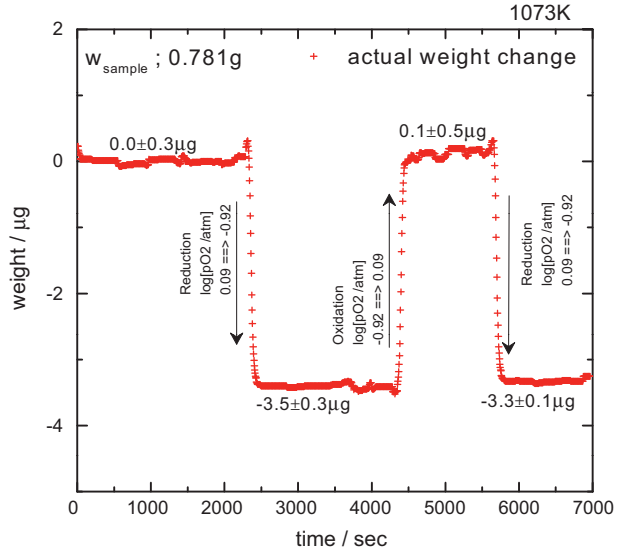

Fig. 3. Typical weight change profile for undoped $BaTiO_{3-\delta}$ upon oxidation and reduction.

On the basis of the defect chemistry with acceptor-type impurity, the nonstoichiometry, δ, which is the deviation from the stoichiometric point ($\delta = 0$), is given over the entire P_{O_2} regime of measurement as [23]

$$\Delta\delta = \delta - \delta^* = -\frac{V_m\sqrt{K_i}}{N_A} \times \sinh\left[\frac{1}{2}\ln\left(1+\frac{2N_A\delta}{V_m[A^{/}]}\right)+\frac{1}{4}\ln\frac{P_{O_2}}{P^o_{O_2}}\right] - \delta^* \quad (4)$$

$$P^o_{O_2} = \left(\frac{2K_{Re}}{[A^{/}]K_i}\right)^2 \quad (5)$$

where δ^* is the oxygen nonstoichiometric value at the starting point of the measurement, V_m the molar volume of the specimen, N_A the Avogadro number, K_i the internal reaction constant, $[A^{/}]$ the acceptor-type cation defect, K_{Re} the external reaction constant, and $P^o_{O_2}$ the P_{O_2} corresponding to the stoichiometric composition ($\delta = 0$) where $n = p = K_i^{1/2}$ for undoped $BaTiO_{3-\delta}$. One should note that the acceptor-type cation defect, $[A^{/}]$, is including cation impurities (Fe, and Al) and cation defects, giving $[A^{/}] = 2[V^{//}_{Ba}] + 4[V^{////}_{Ti}] + [A^{/}_C]$. Particularly, the isotherm relationship between the degree of nonstoichiometric variation and P_{O_2}, which belongs to the disorder

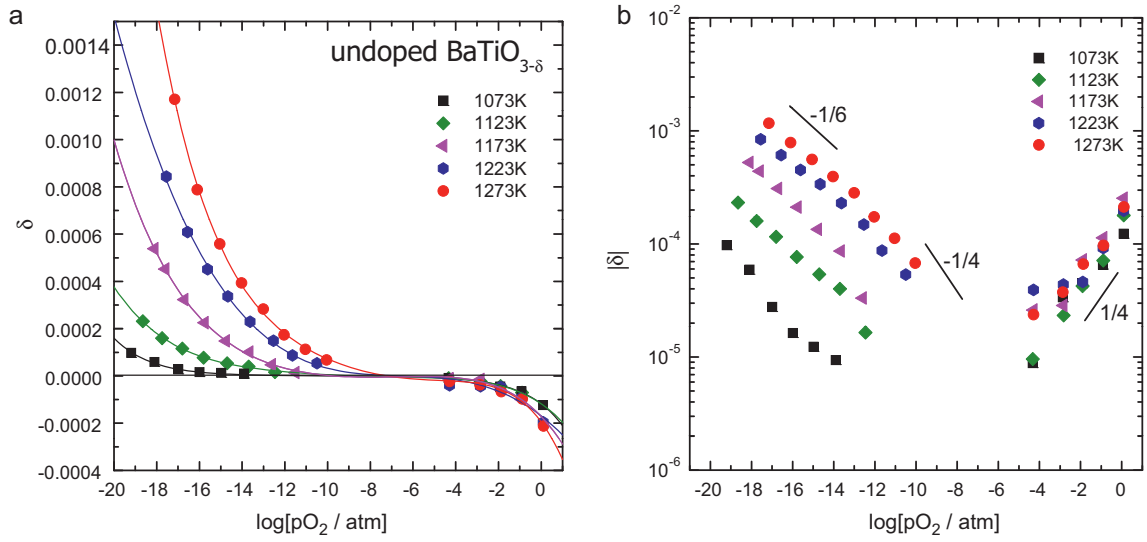

Fig. 4. (a) Oxygen nonstoichiometry, δ, vs. $\log(P_{O_2}/\text{atm})$, (b) $\log\delta$ vs. $\log(P_{O_2}/\text{atm})$ for undoped $BaTiO_{3-\delta}$ of 99.99% purity at different temperatures.

regime of oxygen vacancies compensated by an acceptor-type defect, may be further simplified to [20]

$$\Delta\delta = \delta - \delta^* = -\frac{V_m\sqrt{K_i}}{N_A}\sinh\left[\frac{1}{4}\ln\frac{P_{O_2}}{P^o_{O_2}}\right] - \delta^* \quad (6)$$

where $2N_A\,\delta/V_m \ll [A^/]$ from Eq. (4).

Because the nonstoichiometric change relative to the reference value δ^*, or $\Delta\delta$ (δ–δ^*), was only measured by TG as a function of P_{O_2} at various temperatures, the absolute nonstoichiometric values should be determined by nonlinear fitting to Eq. (4) or (6). By locating an inflection point from a nonstoichiometry isotherm datum which falls at the stoichiometric composition, absolute values for nonstoichiometry may be determined and thermodynamic quantities may be calculated, as has been widely discussed in detail [20,23]. The solid lines in Fig. 4(a) are the best that can be fitted to Eq. (4) with the fitting parameters, K_i, δ^*, and $P^o_{O_2}$, $[A^/]$ at different temperatures. Because Eq. (4) contains the absolute nonstoichiometric values for the corresponding P_{O_2}, first the nonstoichiometric change with P_{O_2} within the n–p transition regime was best fitted with Eq. (6) to get the initial values of K_i, δ^*, and $P^o_{O_2}$. Then, by using these values as starting values, Eq. (6) was numerically fit to the experimental data to obtain full information of the fitting parameters, as shown in Fig. 4(a). The best estimated values by nonlinear fitting of Eq. (4) to the experimental data are summarized in Table 1. The impurity level $[A^/]$ turned out to be constant over the measured temperature, unlike the literature value that was thermally activated with an activation energy of 1.5 eV [23]. This temperature independent property should be understood by either the fixed valence acceptor-type defect including Schottky-Wagner defects, but we could not identify further which one is dominant. Unlike previous TGA studies [11,24–26], the absolute nonstoichiometric values and the stoichiometric point at each temperature ($P^o_{O_2}$) could be successfully calculated due to the high resolution of our TGA, thus providing a more precise understanding of the defect-structrue of $BaTiO_{3-\delta}$. The continuous nature of the isothermal nonstoichiometry, δ, indicated that our measurement was performed for the single phase of $BaTiO_{3-\delta}$. The δ values increased with increasing temperature, and with decreasing a_{O_2} in the low P_{O_2} oxygen deficient regime ($\delta > 0$) in which the endothermic external reaction may be expected. Above the n–p transition point, the oxygen excess regime ($\delta < 0$) was clearly located, although the nonstoichiometric change was small at around 10^{-4} mol. The relationship of $\log|\delta|$ vs. $\log P_{O_2}$, as shown in Fig. 4(b), can be divided into two regions. Below $P_{O_2} \le 10^{-12}$ atm at 1273 K, the oxygen exponent at the isothermal condition, $\delta \propto P^m_{O_2}$, tended close to $m = 1/6$ as the oxygen activity decreased, and sine hyperbolically decreased and increased above $P_{O_2} \ge 10^{-12}$ atm, which was expected from the equilibrium defect diagram where oxygen ionic conductivity remained nearly independent of P_{O_2}. The opposite different slopes across the stoichiometry point may be understood by the change from electron-consuming oxidation to hole-producing oxidation reaction with increasing P_{O_2} [23].

The nonstoichiometric oxygen contents of $BaTiO_{3-\delta}$ at near 1273 K in the literature with different impurity levels and measurement methods [10,11,20,24,25] are plotted in Fig. 5, showing wide scattering oxygen nonstoichiometry. The overall trends of our nonstoichiometric values against oxygen partial pressure were in good agreement, although showing slightly lower than that from coulometric titration with similar purity starting material. Because

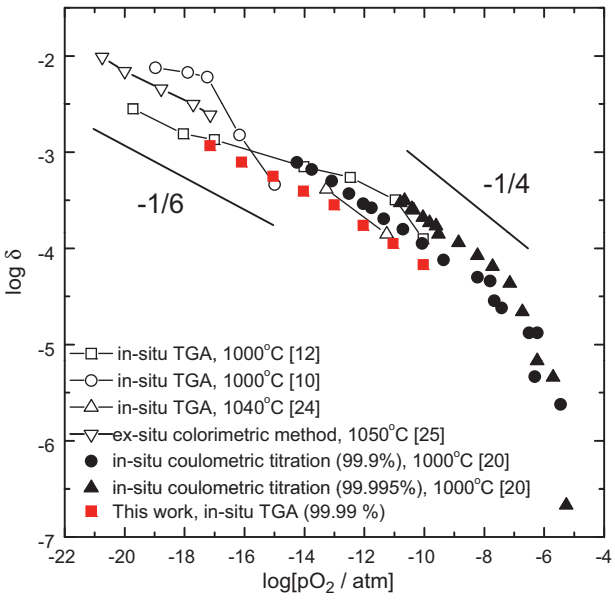

Fig. 5. Comparison of oxygen nonstoichiometry, δ, vs. $\log(P_{O_2}/\text{atm})$ for undoped $BaTiO_{3-\delta}$ with different impurity levels at 1273 K.

Table 1
The best estimated values for K_i, K_{Re}, δ^*, $pO^o{}_2$ and $[A^/]$ for undoped $BaTiO_{3-\delta}$.

Temp.	$\log[K_i/cm^{-6}]$	$\log[pO^o{}_2/atm]$	δ^*	$\log[K_{Re}/cm^{-9}\ atm^{1/2}]$	$\log[[A^/]/cm^{-3}]$
1000 °C	34.52 ± 0.11	−6.11 ± 0.14	−2.15 ± 0.12E-4	50.5 ± 0.32	19.03 ± 0.11
950 °C	34.04 ± 0.10	−6.59 ± 0.05	−1.96 ± 0.15E-4	49.93 ± 0.59	19.01 ± 0.05
900 °C	33.69 ± 0.15	−7.50 ± 0.22	−2.39 ± 0.45E-4	48.97 ± 0.58	19.02 ± 0.08
850 °C	33.15 ± 0.08	−8.70 ± 0.04	−1.78 ± 0.30E-4	47.8 ± 0.64	19.00 ± 0.04
800 °C	32.27 ± 0.14	−9.74 ± 0.09	−1.23 ± 0.03E-4	–	–

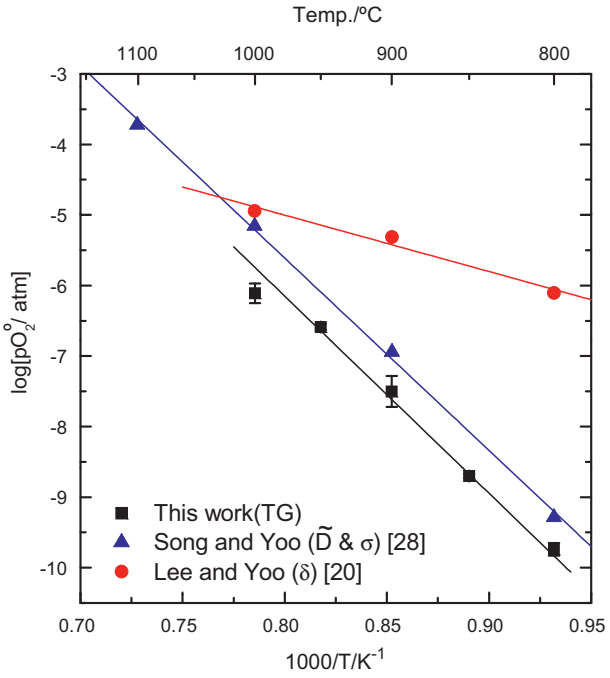

Fig. 6. Comparison of $\log(P_{O_2}/atm)$ for undoped $BaTiO_{3-\delta}$ with the literature.

of the missing information on the cation nonstoichiometry for each measurement, further comparison could not be made here.

Fig. 6 shows the variation of $P^o_{O_2}$, an electronic stoichiometric point, as extracted from our nonstoichiometric data as a function of reciprocal temperature, together with the literature values extracted from coulometric titration [20] and conductivity minimum measurements [28]. Our results are one or two orders of magnitude lower than the previously reported corresponding values, at all measured temperatures. This discrepancy was attributed to the dependency of the n–p transition point on the electron concentration and on the cation nonstoichiometry [27]. However, because negatively charged cation vacancies and electron/hole concentrations may play different roles in the shift of the n–p transition point, these two effects should be considered separately. With increasing electron concentration at a fixed cation ratio, the n–p transition point ($P^o_{O_2}/atm$) moves toward higher P_{O_2} because of the endothermic external reaction, as in the case of our results. As predicted from the literature [27], there is a clear shift of the n–p transition point with deviation of the A/B cation ratio from unity in ABO_3 perovskite. With increasing concentration of negatively charged cation vacancies, the compensation for this excess negative charge results in a corresponding increase in hole or oxygen vacancy concentration. Therefore, the n–p transition point ($P^o_{O_2}/atm$) moves toward lower P_{O_2} with increasing cation nonstoichiometry. Therefore, the difference in stoichiometric P_{O_2} among the different specimens may be understood both by the initial cation nonstoichiometry and the value of external reaction constants including the redox reaction of impurity defect.

The values of the internal reaction constant were plotted against reciprocal temperature, compared with the literature values [12,20,28,30,31] in Fig. 7(a), and found to be best represented as

$$K_i/cm^{-6} = (1.69 \pm 1.51) \times 10^{46}\ \exp\left(-\frac{2.93 \pm 0.23\,eV}{kT}\right) \quad (7)$$

over the entire temperature range. The best estimates are summarized and compared in Table 2. Interestingly, our K_i values are in between the literature values extracted from coulometric titration and conductivity combined with chemical diffusivity or thermopower measurements, even though every value is within the uncertainty level. By considering that the values calculated from the conductivity were evaluated on the basis of several assumptions, including the density of state and carrier mobility, the comparison with the K_i value extracted from nonstoichiometric measurements seemed more reliable and showed very good agreement in terms of activation enthalpy. The small difference may be understood by the impurity level and cation nonstoichiometry of the specimen.

The values of the external reaction constant were plotted against reciprocal temperature in Fig. 7(b), and found to be best represented as

$$K_{Re}/cm^{-9} = (7.15 \pm 5.55) \times 10^{73}\ \exp\left(-\frac{5.80 \pm 0.15\,eV}{kT}\right) \quad (8)$$

over the entire measured temperature range. All the values [20,24,30–32] for K_{Re} reported on undoped $BaTiO_{3-\delta}$, along with the present one, are listed in Table 3 and compared in Fig. 7(b). No assumption regarding on the mobility of the electrical charge carrier or extension from a fixed electro-neutrality regime was made in this analysis. The activation energy was around 5.80 eV, which is in good agreement with the literature values.

Table 2
K_i values with literature data.

Author(s)	K_i/cm^{-6}	Measurement	Ref.
This work	$1.69 \times 10^{46}\ \exp\left(-\frac{2.93\pm0.23\,eV}{kT}\right)$	Nonstoichiometry	–
Song and Yoo	$1.06 \times 10^{45}\ \exp\left(-\frac{3.15\pm0.39\,eV}{kT}\right)$	Conductivity, chemical diffusivity	[28]
Lee and Yoo	$1.08 \times 10^{46}\ \exp\left(-\frac{2.82\pm0.32\,eV}{kT}\right)$	Nonstoichiometry	[20]
Kim et al.	$6.80 \times 10^{44}\ \exp\left(-\frac{2.90\,eV}{kT}\right)$	Conductivity, thermoelectric power	[26]
Seuter	$3.96 \times 10^{46}\ \exp\left(-\frac{3.15\,eV}{kT}\right)$	Conductivity, thermoelectric power	[24]
Nowotny and Rekas	$8.55 \times 10^{44}\ \exp\left(-\frac{2.91\,eV}{kT}\right)$	Conductivity, thermoelectric power	[29]

Table 3
K_{Re} values with literature data.

Author(s)	$K_{Re}/cm^{-9}\ atm^{1/2}$	Defect model	Measurement	Ref.
This work	$7.15\times10^{73}\ \exp\left(-\frac{5.80\pm0.15\,eV}{kT}\right)$	$n+[A^{/}]=2[V_O^{\bullet\bullet}]+p$	Nonstoichiometry	–
Yoo and Song	$3.06\times10^{77}\ \exp\left(-\frac{7.30\pm0.04\,eV}{kT}\right)$	$n+[A^{/}]=2[V_O^{\bullet\bullet}]+p$	Conductivity, chemical diffusivity	[30]
Chan et al.	$7.09\times10^{70}\ \exp\left(-\frac{5.89\,eV}{kT}\right)$	$n+[A_C^{/}]=2[V_O^{\bullet\bullet}]$	Conductivity	[31]
Seuter	$1.30\times10^{72}\ \exp\left(-\frac{5.70\,eV}{kT}\right)$	$[V_{Ba}^{//}]=2[V_O^{\bullet\bullet}]+p$	Conductivity	[24]
Daniels and Härdtl	$2.56\times10^{71}\ \exp\left(-\frac{6.10\,eV}{kT}\right)$	$[V_{Ba}^{//}]=2[V_O^{\bullet\bullet}]+p$	Conductivity	[32]
Nowotny and Rekas	$1.06\times10^{71}\ \exp\left(-\frac{5.69\,eV}{kT}\right)$	$[V_{Ba}^{//}]=2[V_O^{\bullet\bullet}]+p$	Conductivity	[29]
Hagemann and Hennings	$9.43\times10^{72}\ \exp\left(-\frac{-5.99\,eV}{kT}\right)$	$n=2[V_O^{\bullet\bullet}]$	Nonstoichiometry	[11]

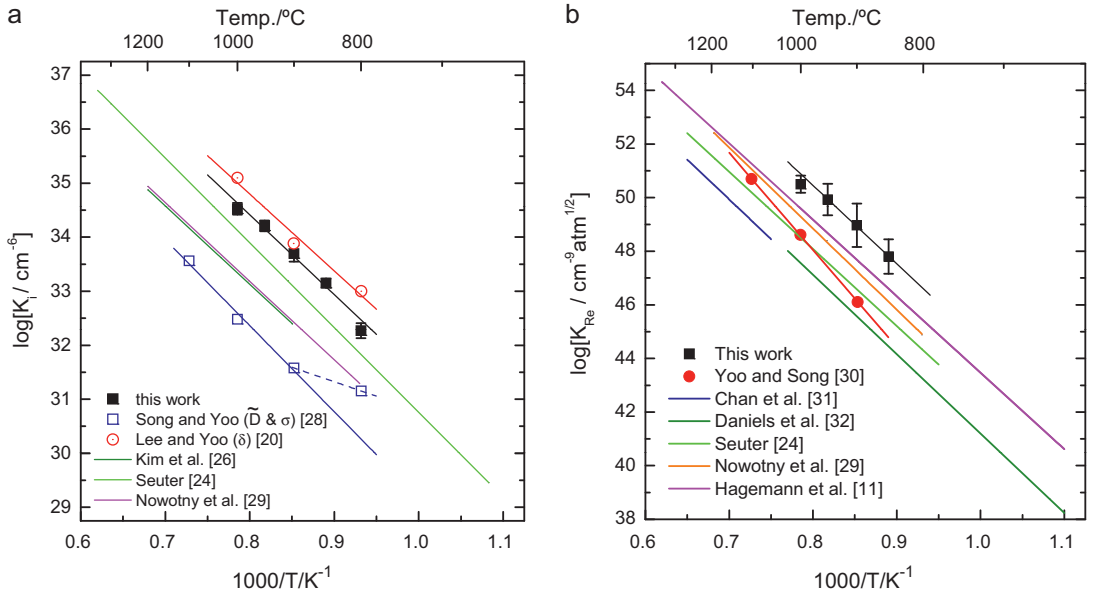

Fig. 7. (a) Comparison of internal reaction constant, K_i, with the literature, and (b) comparison of external reaction constant, K_{Re}, with the literature for undoped $BaTiO_{3-\delta}$.

Because of the solid/gas equilibrium criterion, the relative partial molar enthalpy, $\Delta\bar{H}_O$, and entropy, $\Delta\bar{S}_O$, of the oxygen component for $BaTiO_{3-\delta}$ are best estimated by linear fitting of Eq. (9) at various oxygen nonstoichiometries [20].

$$\ln P_{O_2} = \frac{2\Delta\bar{H}_O}{RT} - \frac{2\Delta\bar{S}_O}{R} \tag{9}$$

where the partial molar enthalpy and entropy for oxygen incorporation are further determined from the nonstoichiometric data using the relation

$$\Delta\bar{H}_O = h_O(\delta) - h_O^o = \frac{R}{2}\frac{d\ \ln P_{O_2}}{d(1/T)}\bigg|_\delta,$$

$$\Delta\bar{S}_O = s_O(\delta) - s_O^o = -\frac{R}{2}\frac{d(T\ \ln P_{O_2})}{dT}\bigg|_\delta \tag{10}$$

From the $\delta - P_{O_2} - T$ relation shown in Fig. 8, where the values of P_{O_2}, corresponding to the same nonstoichiometry at different temperatures, were obtained by solving Eq. (4) with the values in Table 1, the calculated relative partial molar enthalpy and entropy of oxygen from the slope and intercept are plotted as a function of oxygen nonstoichiometry in Fig. 9. The negative sign of $\Delta\bar{H}_O$ and $\Delta\bar{S}_O$ in the oxygen deficient regime indicates that the incorporation of oxygen is an exothermic process, whereas the endothermic process in the oxygen excess regime was confirmed by the positive sign of $\Delta\bar{H}_O$ and $\Delta\bar{S}_O$. The asymmetric oppositely signed values for oxygen excess and deficient regimes for both partial molar enthalpy and entropy of oxygen were discussed in terms of the transition

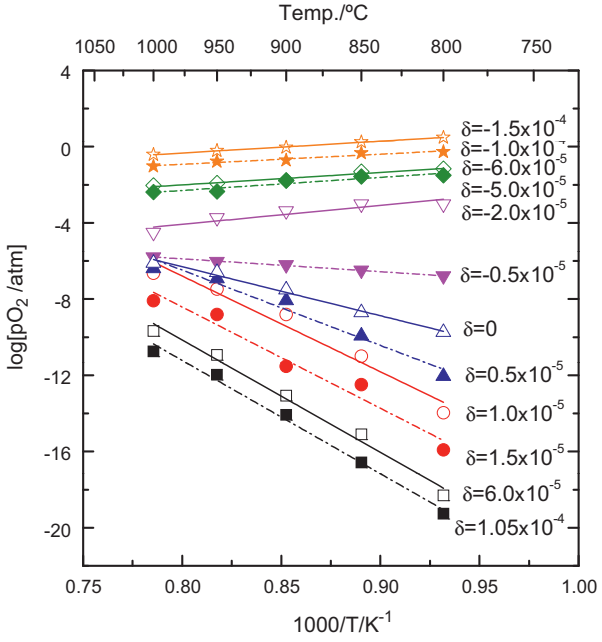

Fig. 8. Equilibrium oxygen activity vs. reciprocal temperature at different nonstoichiometry for undoped $BaTiO_{3-\delta}$.

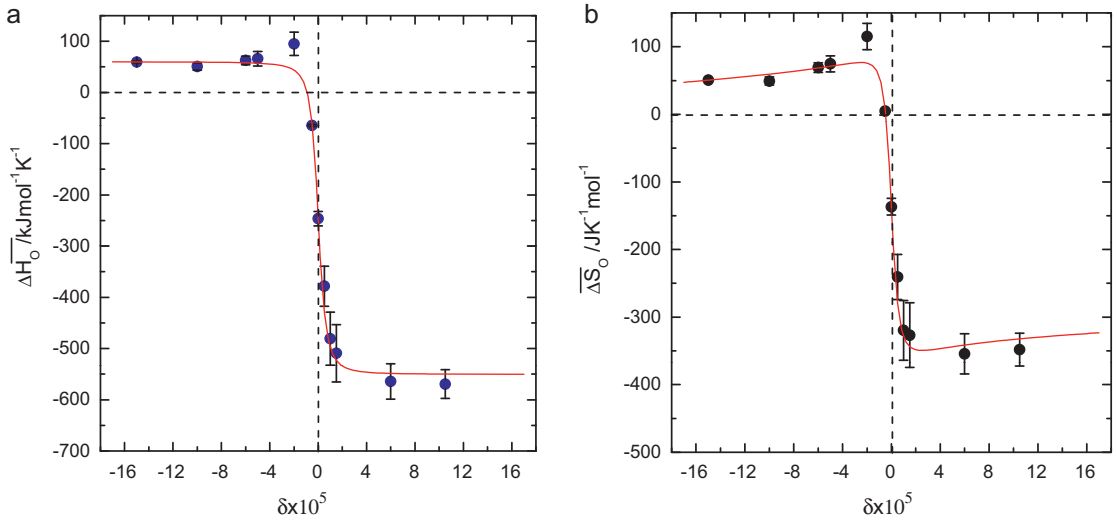

Fig. 9. (a) Relative partial molar enthalpy, $\Delta\bar{H}_O$, of oxygen vs. nonstoichiometry, and (b) relative partial molar entropy, $\Delta\bar{S}_O$, of oxygen vs. nonstoichiometry for undoped $BaTiO_{3-\delta}$.

of oxygen incorporation reactions across the stoichiometric point from electron consuming to hole producing external reaction:

$$\frac{1}{2}O_2(g) + V_O^{\bullet\bullet} = O_O^x + 2h^{\bullet}; \quad (11\text{-a})$$

$$\frac{1}{2}O_2(g) + V_O^{\bullet\bullet} + 2e^{/} = O_O^x; \quad (11\text{-b})$$

Therefore, the partial molar enthalpy of oxygen in n to p transition regime should be given as the fractional sum of $\Delta\bar{H}_O(p)$, and $\Delta\bar{H}_O(n)$, due to Eqs. (3) and (4)

$$\begin{aligned}\Delta\bar{H}_O &= \frac{n}{n+p}\Delta\bar{H}_O(n) + \frac{p}{n+p}\Delta\bar{H}_O(p)\\ &= \frac{1}{2}[\Delta\bar{H}_O(n) + \Delta\bar{H}_O(p)]\\ &\quad - \frac{\beta\delta}{2[(\beta\delta)^2 + 4K_i]^{1/2}}\cdot[\Delta\bar{H}_O(p) - \Delta\bar{H}_O(n)]\end{aligned} \quad (12)$$

with $\beta = 2N_A/V_m$. As shown in Fig. 9(a), the variation of partial molar enthalpy of oxygen across the stoichiometry point is fitted to Eq. (12), giving the saturation value of *ca.* −580 kJ/mol in the oxygen excess regime and *ca.* 52 kJ/mol in the oxygen deficient regime. A similar trend was observed in the partial molar entropy of oxygen, as shown in Fig. 9(b). By same argument, the result is as depicted by the solid curve in Fig. 9(b) with the best estimated values.

$$\begin{aligned}\Delta\bar{S}_O(\delta)/\mathrm{J\ K^{-1}\ mol^{-1}} &= (-59.6 \pm 10.7) + R\ln\frac{(\delta + x/2)}{(3 - \delta - x/2)}\\ &\quad - \frac{(256.2 \pm 8.5)\delta}{[\delta^2 + (4.5 \pm 0.5)\times 10^{-11}]^{1/2}}\\ &\quad + R\ln\left\{\frac{\delta + [\delta^2 + (4.5 \pm 0.5)\times 10^{-11}]^{1/2}}{-\delta + [\delta^2 + (4.5 \pm 0.5)\times 10^{-11}]^{1/2}}\right\}\end{aligned} \quad (13)$$

4. Conclusion

On the basis of the defect chemistry by introducing the acceptor-type defect including cation nonstoichiometry and impurities, oxygen nonstoichiometry of $BaTiO_{3-\delta}$, δ, was successfully determined with non-linear functional fitting by using the best estimated values of K_{Re}, K_i, δ^*, $P^o_{O_2}$, and $[A^{/}]$ for 99.99% pure $BaTiO_{3-\delta}$. Our values for K_i and K_{Re} of the undoped $BaTiO_{3-\delta}$ were are best described by the following equations:

$$K_i/\mathrm{cm^{-6}} = (1.69 \pm 1.51)\times 10^{46}\ \exp\left(-\frac{2.93 \pm 0.23\,\mathrm{eV}}{kT}\right)$$

$$K_{Re}/\mathrm{cm^{-9}} = (7.15 \pm 5.55)\times 10^{73}\ \exp\left(-\frac{5.80 \pm 0.15\,\mathrm{eV}}{kT}\right),$$

and the difference compared with reference data should be further understood by identifying the cation nonstoichiometry and the value of impurity defects for the clarification of defect structure.

The relative partial molar enthalpy and entropy of oxygen for undoped $BaTiO_{3-\delta}$ were also calculated and the asymmetric oppositely signed values for oxygen excess and deficient regimes for both partial molar enthalpy and entropy of oxygen were discussed in terms of the transition of oxygen incorporation reactions from electron consuming to hole producing external reaction across the stoichiometric point.

Acknowledgments

This work was supported by the Basic Research Laboratories Program through the National Research Foundation of Korea (NRF) funded by the Ministry of Education, Science and Technology (2009-0085441).

References

[1] H.L. Tuller, in: O.T. Sorensen (Ed.), Nonstoichiometric Oxides, Academic Press, New York, 1981, pp. 271–335.
[2] F.A. Kroger, V.J. Vink, in: F. Seitz, D. Turnbull (Eds.), Solid State Physics, vol. 3, Academic Press, New York, 1956, pp. 307–435.
[3] G.W. Castellan, Physical Chemistry, third ed., University of Maryland, College Park, MD, 1957, p. 85.
[4] N.J. Field, A.P. DeBretteville, H.D. Williams, Phys. Rev. 72 (1947) 1119–1120.
[5] M. Schrader, D. Mienert, T.-S. Oh, H.-I. Yoo, K.D. Becker, Solid State Sci. 10 (2008) 768–775.
[6] C.-E. Lee, H.-I. Yoo, Solid State Ionics 179 (2008) 338–346.
[7] R. Wernicke, Phys. Stat. Sol. 47 (1978) 139–144.
[8] J. Mizusaki, Y. Mima, S. Yamauchi, K. Fueki, J. Solid State Chem. 80 (1989) 102–111.
[9] R. Dieckmann, Ber. Bunsenges. Phys. Chem. 86 (2) (1982) 112–118.
[10] R.J. Panlener, R.N. Blumenthal, J. Am. Ceram. Soc. 54 (1971) 610–613.
[11] R. Dieckmann, Z. Phys. Chem. NF 107 (2) (1977) 189–210.
[12] H.-J. Hagemann, D. Hennings, J. Am. Ceram. Soc. 64 (1981) 590–594.
[13] H.-I. Yoo, C.-E. Lee, J. Am. Ceram. Soc. 88 (2005) 617–623.
[14] E. Robens, Vacuum Microbalance Tech. 9 (1969) 73–95.

[15] W. Kuhn, E. Robens, G. Sandstede, G. Walter, Vacuum Microbalance Tech. 10 (1970) 160–172.
[16] R. Dieckmann, Philos. Mag. 68 (4) (1993) 725–745.
[17] T. Steensland, K.S. Forland, Vacuum Microbalance Tech. 5 (1966) 17–31.
[18] R.A. Pierotil, Vacuum Microbalance Tech. 5 (1966) 1–15.
[19] J.A. Poulis, J.M. Thomas, Vacuum Microbalance Tech. 1 (1962) 1–14.
[20] D.-K. Lee, H.-I. Yoo, Solid State Ionics 144 (2001) 87–97.
[21] J. Nowotny, M. Rekas, Ceram. Int. 20 (1994) 265–275.
[22] R. Wernicke, Philips Res. Rep. 31 (1976) 526–543.
[23] H.-I. Yoo, C.-R. Song, D.-K. Lee, J. Electroceram. 8 (2002) 5–36.
[24] A.M.J.H. Seuter, Philips Res. Rep. Suppl. 3 (1974) 1–84.
[25] G.V. Bois, N.A. Mikhailova, E.I. Prodavtsova, V.A. Yusova, News Acad. Sci. USSR Inorg. Mater. (1976) 1302–1305.
[26] J.-Y. Kim, C.-R. Song, H.-I. Yoo, J. Electroceram. 1 (1997) 27–35.
[27] S.-J. Song, E.D. Wachsman, S.E. Dorris, U. Balachandran, Solid State Ionics 149 (2002) 1–10.
[28] C.-R. Song, H.-I. Yoo, Phys. Rev. B 61 (2000) 3975–3982.
[29] J. Nowotny, M. Rekas, Ceram. Int. 20 (1994) 225–235.
[30] H.-I. Yoo, C.-R. Song, Electrochemistry 68 (6) (2000) 415–422.
[31] N.-H. Chan, R.K. Sharma, D.M. Smyth, J. Am. Ceram. Soc. 65 (1982) 167–170.
[32] J. Daniels, K.H. Hardtl, Philips Res. Rep. 31 (1976) 489–504.